Journal Pre-proof

Confinement of MWCNTs in PA6 3D-printed fibreglass-reinforced composites to enhance piezoresistive properties

Nicolò Geneletti , Gennaro Rollo , Luca Michele Martulli , Andrea Bernasconi , Alfredo Ronca , Andrea Sorrentino , Marino Lavorgna

PII: S2666-6820(25)00134-3
DOI: https://doi.org/10.1016/j.jcomc.2025.100692
Reference: JCOMC 100692

To appear in: *Composites Part C: Open Access*

Received date: 26 September 2025
Revised date: 24 November 2025
Accepted date: 31 December 2025

Please cite this article as: Nicolò Geneletti , Gennaro Rollo , Luca Michele Martulli , Andrea Bernasconi , Alfredo Ronca , Andrea Sorrentino , Marino Lavorgna , Confinement of MWCNTs in PA6 3D-printed fibreglass-reinforced composites to enhance piezoresistive properties, *Composites Part C: Open Access* (2026), doi: https://doi.org/10.1016/j.jcomc.2025.100692

Confinement of MWCNTs in PA6 3D-printed fibreglass-reinforced composites to enhance piezoresistive properties

Nicolò Geneletti[1], Gennaro Rollo[2*], Luca Michele Martulli[1], Andrea Bernasconi[1], Alfredo Ronca[3], Andrea Sorrentino[2,3], Marino Lavorgna[2,3]

[1]Department of Mechanical Engineering, Politecnico di Milano, Via La Masa 1, I-20156 Milano, Italy
[2]Polymer, Composites and Biomaterials Institute, National Research Council (CNR), P.le Fermi 1, 80055 Portici (NA), Italy
[3]Polymer, Composites and Biomaterials Institute, National Research Council (CNR), Via Previati 1/E, 23900 Lecco (LC), Italy

[*]corresponding author

Abstract

A continuous fibreglass (CFG)-reinforced polyamide 6 (PA6) sandwich structure with self-sensing capabilities was developed by confining multi-walled carbon nanotubes (MWCNTs) within the material volume through a step-by-step process involving a) 3D printing of specimens with a designed porous structure, b) embedding MWCNTs onto the surface of polyamide pores swollen with acid-formic solutions containing various filler contents, and c) hot-pressing the resulting specimens to close the porosity. Sandwiched specimens, designed with top-bottom skins at control layup (no reinforcement CFG, namely "noGF"), the quasi-isotropic (with CFG oriented 0/45/90/-45°s, namely "qiGF"), and the longitudinal layup (with CFG oriented at 0°, namely "longGF") were subjected to steady and cyclic three-point bending tests and mechanical and piezoresistive characterized. The results show a correlation between applied strain and measured electrical resistance, with a gauge factor (GF) of 23 at a strain of 0.83% for the sample containing 0.05 wt% MWCNTs. The fibre reinforcement, together with the porous sandwich design, proved effective in reducing electrical hysteresis and improving measurement repeatability. The sample containing 0.05 wt% of MWCNTs and longGF shows a significant improvement in sensing performance. These findings confirm that confining

MWCNTs within 3D-printed PA6 sandwich structures is an effective strategy for enhancing the piezoresistivity.

Keywords: fused deposition modelling (FDM); multi-walled carbon nanotube (MWCNT); fibre-reinforced composite (FRC); structural health monitoring; strain sensors.

Abbreviations

The following abbreviations are used in this manuscript:

AM	Additive Manufacturing
CAD	Computer Aided Design
CFG	Continuous Fibreglass
CNT	Carbon Nanotube
CPC	Conductive Polymer Composite
CTAB	Cetyltrimethyl-Ammonium Bromide
DSC	Differential Scanning Calorimetry
FDM	Fused Deposition Modelling
FRC	Fibre-Reinforced Composite
GF	Gauge Factor
H_2O	Water
MWCNT	Multi-Walled Carbon Nanotube
MWCNTs	Multi-Walled Carbon Nanotubes
PA6	Polyamide 6
RMSE	Root-Mean-Square Error
SEM	Scanning Electron Microscope / Microscopy
SHM	Structural Health Monitoring
T_g	Glass Transition Temperature
T_m	Melting Temperature
WR	Working Range
noGF	No Glass Fibre reinforcement
qiGF	Quasi-Isotropic Glass Fibre reinforcement
longGF	Longitudinal Glass Fibre reinforcement

1 Introduction

In recent years, composite materials have become the preferred choice for a wide range of applications due to their exceptional thermal, electrical, and mechanical performance, as well

as their lightweight [1]. During service, composite structures must be monitored to detect cracks and other damage-related issues. Structural health monitoring (SHM) enables real-time condition assessment of such structures, but it often requires complex sensor networks and can lead to weight increase or even a loss of mechanical properties when sensors are embedded or attached [2], [3], [4].

Due to these limitations, there is growing interest in designing structured materials capable of sensing their own condition without external sensors. Self-sensing materials may be engineered to monitor stress, strain, damage, or temperature changes by tracking variations in their electrical properties [3], [4], [5]. These materials eliminate the need for implanted sensor systems, leading to lower costs, higher durability, larger sensing volumes, and less degradation of mechanical properties [6]. In this context, conductive polymer composites (CPCs), formed by adding conductive fillers to a polymer matrix, are of particular interest for strain self-sensing. Common fillers include graphene nanoplatelets [5], [7], [8], carbon black [9], [10], carbon nanotubes [11], [12], [13], and metallic particles [14], [15]. Among these, MWCNTs stand out due to their high aspect ratio, which facilitates the formation of extensive conductive networks at low loadings [14], [16]. Consequently, MWCNTs are considered highly effective fillers for strain-sensing applications [17]. Moreover, MWCNTs offer several advantages, including simpler prototype design, ease of achieving homogeneous dispersion, and efficient interfacial interaction between filler and matrix. [18]. Generally, CPCs can be synthesized using two different approaches [11]: either by homogeneously dispersing filler particles within the volume matrix or by creating a segregated structure through the confinement of filler in a selected volume partition. The latter method generally enables percolation at a lower filler concentration compared to geometrical percolation, as electrical conduction mainly occurs through direct contact between conductive particles rather than electrons tunneling. Several techniques have been developed in recent years to obtain conductive segregated structures, including self-

assembly latex mixing, blending of immiscible phases, and solid or porous phase exclusion [19].

Additive manufacturing (AM) is a process that builds a component layer-by-layer starting from digital data [20], with the possibility to combine porosity and fiber reinforced layers in sandwich structures. Among the various AM methods available [21], [22], [23], Fused Deposition Modelling (FDM) is one of the most widely used in prototyping [24], and has recently been explored for the possibility of embedding continuous fibres directly into the printed object. This technology enables the production of composite materials with a notable improvement in their mechanical properties [25], [26], [27], [28], [29]. The presence of continuous fibres broadens the versatility of the fabricated structures which can ultimately be used for self-sensing or self-monitoring applications [30]. Wang et al. [31] recently investigated a structure fabricated by using carbon nanotubes and polylactic polymer and a FDM 3D-printing approach to promove the confinement. An aqueous dispersion of carbon nanotubes (CNTs) was prepared using cetyltrimethyl-ammonium bromide (CTAB) as surfactant, which was later used in the bath-coating of the porous printed structure. The specimen then underwent a hot compression stage, which promoted the segregation of the carbonaceous filler within the sample volume, thereby enhancing its shielding properties against electromagnetic interference.

Inspired by that approach, this study explores for the first time the confinement of MWCNTs within a fiberglass-reinforced, 3D-printed PA6 porous sandwich structure for strain-sensing applications. The aim is to optimize the electrical conductivity of MWCNT-based composites by examining the influence of filler content, polyamide swelling, and the confinement of nanotubes within the engineered porosity to achieve continuous, efficient electrical pathways and reliable strain-sensing performance.

2 Materials and methods

The printer used was an Onyx Pro (Markforged, Waltham, USA). The filament material, Onyx [32], purchased from Markforged, is a polyamide-6 (PA6) reinforced with 10% short carbon fibers. The spool was dehumidified in an oven at 55 °C for 20 h and stored in a dry box during printing. The fibreglass-reinforced spool was also purchased from Markforged. The extrusion temperatures were set to 275 °C for the polymer nozzle and 252 °C for the continuous fiber nozzle, according to the printer settings. The chemicals were purchased from Avantor (Radnor Township, USA), while the MWCNTs were NC7000 purchased from NANOCYL (Sambreville, Belgium).

2.1 Preliminary swelling test

A preliminary swelling test was conducted to examine the effect of formic acid on the Onyx PA6 material and to select a suitable formic-acid concentration able to facilitate the embedding of MWCNTs onto the printed composite structures (as exhaustively described later). Five acid concentration levels were evaluated: 88% v/v (from literature [33]), 60%, 40%, 20% and 0% v/v (water, control). Twentyfive segments of Onyx filament were cut from the 3D printing spool and dried for 24 hours at 65 °C under 0.1 bar of vacuum to evaporate any absorbed moisture. Each fragment was then weighed on a Dab 100-3 digital scale (Kern, Balingen, Germany) and immersed in the acid solution. Five fragments were tested for each concentration level. The weight of each filament was recorded every 20 minutes, followed by additional measurements every 60 minutes. The weights were normalized relative to their initial values (pre-acid bath). By analyzing the weight evolution of each filament, the acid uptake and the dissolving effect of formic acid on the PA6 material were assessed. Results show that at acid concentrations above 60% v/v the material quickly dissolves (Figure S1). Whereas the sample at control set (i.e. 100% H_2O) remained close to its original weight and only absorbed a small amount of

water. At 40% v/v and 20% v/v acid concentrations, the formic acid allowed Onyx to swell, and uptake more acid mass compared to the control set (see Figure 1). In particular, 40% v/v acid allows for the maximum acid uptake. Therefore, this acid concentration was selected for realising MWCNTs dispersions which were used for the embedding of carbon nanotubes within the polyamide 3D printed samples.

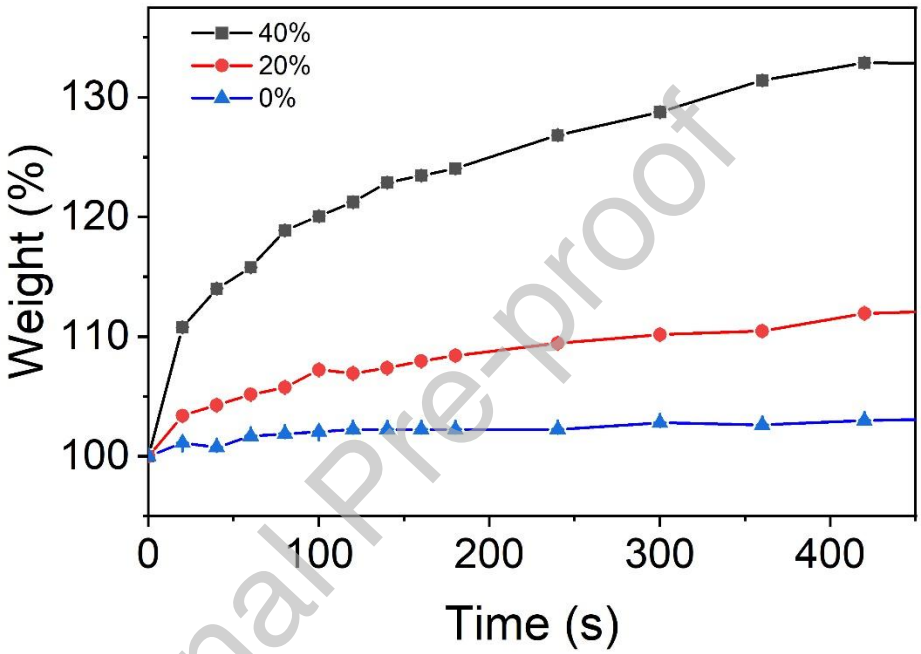

Figure 1. Weight uptake during swelling tests for PA-6 in water (blue) and formic acid solution at 20% v/v (red), and 40% v/v (black).

2.2 Specimen design and manufacturing process

The composites specimens consisted of a rectangular-based prism sandwich structure with dimensions 100×20×9 mm^3, considering its final values (after the hot-press step). The manufacturing process starts with the design and fabrication of 3D printed structures, with designed pores, used to promote the confinement of MWCNTs in a restrict volume of the resulting composite specimens. For the sample to be printed, the thicknesses were set at 1 mm

for the top skin reinforced with fiberglass, 2 mm for the internal channels, and 7.5 mm for the infill and the bottom skin (Figure 2). The channels, necessary to promote the MWCNTs confinement, were positioned at a set distance from the neutral axis in order to maximize the strain to which the confined MWCNTs will be subjected under a bending load.

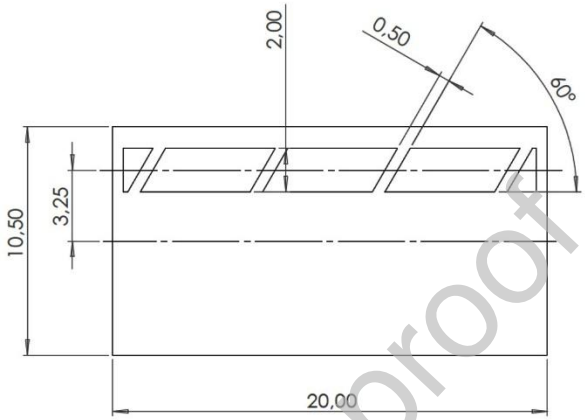

Figure 2. Frontal design of specimen in the printed configuration (before the hot-press step), with the dimensions indicated in mm.

Solidworks 2022 SP02 (30.2.0.46, Dassault Systemes', Vélizy-Villacoublay, France) was used to design the Computer Aided Design (CAD) specimen. The 3D model was then exported into Eiger.io (v3.20.3, Markforged, Waltham, USA) where the default slicing settings include: 0.1 mm of layer height, a triangular fill pattern, 37% of fill density, 3 roof and floor layers, and 2 wall layers. Four layers of continuous fibre per each skin were generated, using the slicer. The reinforcement fibres were localized in the skins of the sandwich structure. In particular, each skin was set to consist of a 0.4 mm core (fibre-reinforcement layers), placed in between 0.3 mm solid polymeric layers. To evaluate the contribution of continuous fibers and their orientation, three configurations were considered: a sample without reinforcement CFG (namely "noGF") used as control, the quasi-isotropic (with CFG oriented 0/45/90/-45°s, namely "qiGF"), and the longitudinal layup (with CFG oriented at 0°, namely "longGF"). The thickness of the specimens

was measured at the end of the manufacturing process, after the hot-press step. The average thickness was of 9.02±0.08 mm.

The MWCNTs confinement inside the pores was achieved in two steps: (1) Slight swelling of the PA6 surface at the printed pores by filling them with a solution containing MWCNTs and allowing the MWCNTs to embed on the surface once the solvent is removed; (2) Compression of the channels using a hot-press, ensuring that the fillers embedded in the polyamide are securely confined. The first step, was performed with dispersions of MWCNTs 0.1 wt%, 0.2 wt%, and 0.5 wt% in a 40% v/v solution of formic acid, which causes the necessary swelling of the polyimide surface [33].

The manufacturing process (schematically summarized in Figure 3) involves the design of a sandwich-like structure, with the skins containing the reinforcing fibers and the pores along the entire length of the sample. The MWCNTs are then deposited on the surface of the pores as well as internally at the channels. After the hot-pressing step, the resulting composite presents a confined MWCNTs structure, which exhibits robust piezoresistive properties.

More experimental details about the several steps of the manufacturing process are reported in the following sections, focusing on a) functionalization of MWCNTs, b) preparation of MWCNTs dispersion in acid-formic 40% v/v solution, c) MWCNTs coating of surface pores and hot-press treatment to obtain the final sandwiched-samples. According with this procedure for each reinforced skin typology (i.e. CFG oriented 0/45/90/-45°s and CFG oriented at 0°) were prepared three composites with three MWCNTs contents equal to 0.03, 0.05, and 0.13 wt% (derivate from dispersion at 0.1, 0.2, and 0.5 wt% of MWCNTs, respectively). According to the previously described nomenclature for CFG orientation and MWCNTs concentration after solvent evaporation, in the specimens are namely following the scheme CFG

orientation/MWCNTs weight percentage (i.e. for the specimens with 0.05 wt% of MWCNTs the name are: noGF/0.05wt%, qiGF/0.05wt%, and longGF/0.05wt%).

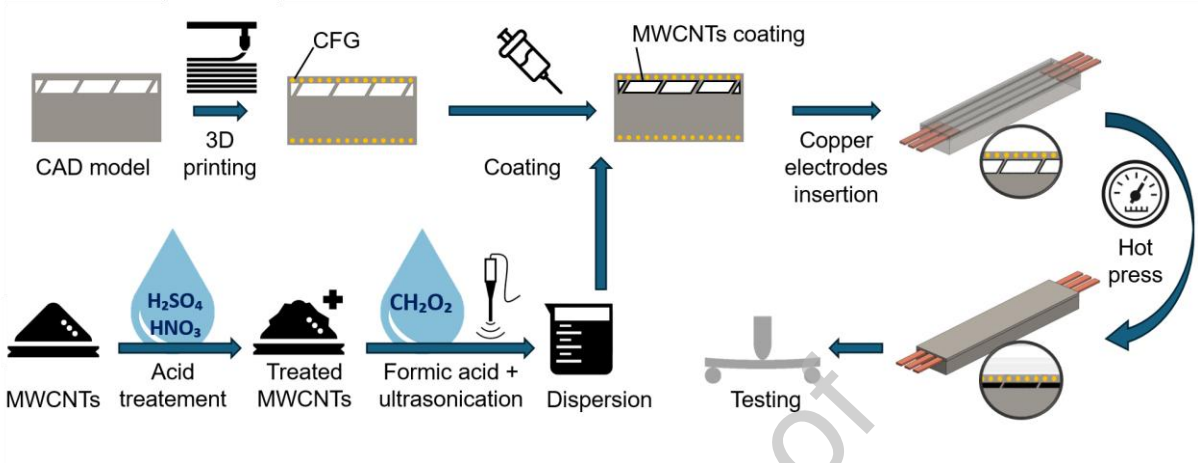

Figure 3. Schematic representation of the manufacturing process.

2.3 MWCNTs sulfonitric treatment

In order to functionalize MWCNTs surface and enhance their dispersibility in water as well as interactions with polyamide, the filler was treated following the procedure suggested by Liu et al. [33] MWCNTs powder was gradually added to a mixture of 95% v/v sulphuric acid and 65% v/v nitric acid (3:1 weight ratio), using a concentration of 0.5wt%. The dispersion was then magnetically stirred at 500 rpm for 18 hours at room temperature using a F20500162 hot plate stirrer (VELP Scientifica, Usmate, Italy). Afterwards, the MWCNTs/acid mixture was diluted with pure water at a 1:20 ratio. The diluted mixture was filtered using a paper filter subject to near-void pressure. The filtration process was carried out in small batches, allowing separation of the liquid acid mixture from the solid carbon nanotubes. The nanotubes were then washed with distilled water until the pH reached 7. The neutral-pH water/nanotubes mixture was filtered again to remove the liquid part. The resulting wet powder was dried in a Vacucell Eco Vacuum Drying Oven (MMM, München, Germany) at 55 °C for 24 h. After drying, the MWCNTs were gently ground into a fine powder using a mortar.

2.4 MWCNTs dispersion preparation

Formic acid-based MWCNTs dispersions, used to treat the surface of the 3D printed structure, consist of 40% v/v formic acid with three different MWCNT concentrations: 0.1 wt%, 0.2 wt%, and 0.5 wt%. The dispersions were magnetically stirred for 30 min and then transferred to the FB505 ultrasonication station (Fisher Scientific, Pittsburgh, USA), and further sonicated for 90 min at room temperature with the aid of an ice bath to avoid excessing temperature raising. The 500 kW, 20 kHz ultrasonicator was set to 40% amplitude with a cycle of 5 seconds on and 3 seconds off.

2.5 MWCNTs coating of the printed porous structure and hot-pressing step

The 3D printed specimen pores were sealed at one end using laboratory wax film (Amcor, Zürich, Switzerland). A Pasteur pipette was then used to fill each channel individually with the selected MWCNTs dispersion from the open end (Figure 4). After filling, the specimens were left to air dry for 24 h. The Parafilm seal was removed and the specimen was placed in an oven for 72 h at 60 °C and 0.1 bar pressure to remove residual of formic acid and water.

Afterwards, the specimens were hot-pressed at high temperatures to reduce internal porosity (i.e., internal pores) and confinate the MWCNTs within the final structure. Simultaneously, the copper electrodes, which were later used for electrical measurement, were fixed in place. As shown in Figure 4, copper electrodes, 8 mm length, were inserted into each internal channel at both ends. The pressing was performed using an AUP10 (Shenzhen Tuopuke Industrial Co., Shenzhen, China) 10-ton electric press, and a custom-milled steel plate was used as the frame for the specimens.

The hot-pressing was carried out at 100 °C for 40 s, then the temperature of the flange closer to the MWCNTs was increased to 210 °C with pressure hold for 15 seconds. The temperature stages were chosen based on Differential Scanning Calorimetry (DSC) analysis, which

identified the glass transition temperature T_g and the melting temperature T_m of the printed material at 73 °C and 215 °C, respectively (Figure S2). After the press was released, each specimen was cooled down to room temperature to minimize the springback in the polymeric material.

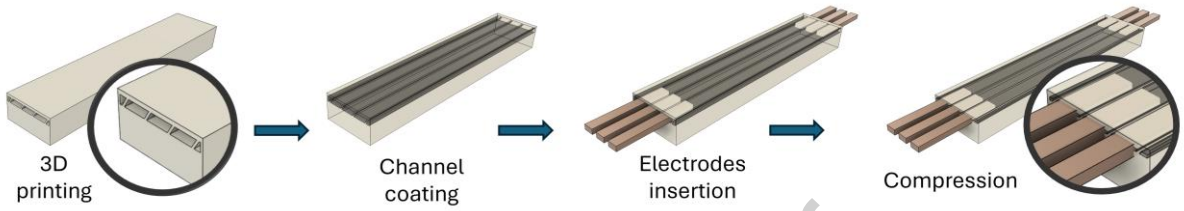

Figure 4. Schematic representation of 3D printed sandwich structure preparation.

2.6 Characterization of the 3D printed samples

The MWCNTs distribution inside the confined volume of 3D printed samples was observed using a Quanta 200 SEM FEG scanning electron microscope (FEI, Hillsboro, USA). The samples were fractured in liquid nitrogen, fixed on a support and metallized with a gold-palladium alloy. The cross section of the specimens was then observed.

The piezoresistive behaviour of the 3D printed samples with the confinement of MWCNTs was tested in the three-point bending configuration. The copper electrodes at each end were connected (Figure 5a), and each specimen was centred on two support wedges, with probes attached to the electrode joints (Figure 5b). Testing was performed using a custom-built LiTeM system, coupled with an RTC-9001 Test Controller (LiTeM, Ancona, Italy), a 200 mm pneumatic actuator, and a 250 kg load cell. Electrical measurements were made using a 2450 SourceMeter (Keithley, Cleveland, USA). The span was set to 80 mm for all tests. Each specimen was preloaded to 30 N. The load pin was then moved to the set point (0.6 mm down). From there, a sinusoidal vertical displacement was applied to the load pin between 0.2 mm and 1.0 mm (0 being the pre-load point). The specimen was tested for 1000 cycles at 0.5 Hz.

Creep/recovery tests were conducted to assess the repeatability and steady-state behavior of the specimens [34]. These tests were performed after the cyclic loading and involved applying alternating displacements over a prolonged period. The testing sequence began with an initial displacement of 1.0 mm held for 10 min, followed by alternating displacements of 0.2 mm and 1.0 mm, each held for 5 min.

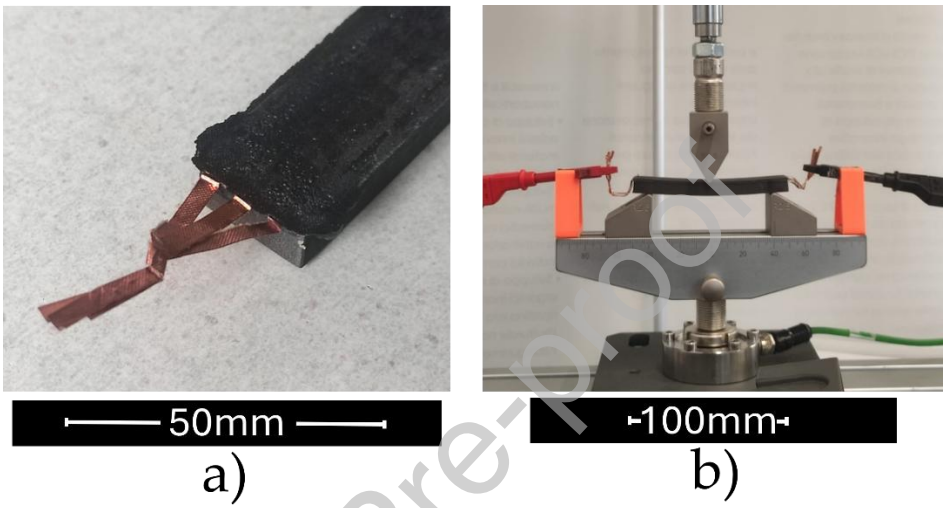

Figure 5. a) The electrodes are joined together at either ends; b) Three-point bending test setup.

3 Results and discussion

The investigation of the confinement of MWCNTs within polyamide-6 (PA6) 3D-printed fiberglass-reinforced composites aimed to evaluate their impact on the material's piezoresistive properties. The integration of MWCNTs within a structured polymer matrix is a promising approach to developing self-sensing materials with enhanced mechanical and electrical performance. To assess these properties, the specimens were subjected to morphological, mechanical, and electrical characterization, focusing on their response under three-point bending tests and cyclic loading conditions.

3.1 Morphological characterization of MWCNTs confinement

SEM images revealed an uneven distribution of carbon nanotubes across the specimen section in samples treated with lower filler content dispersions (Figure 6a), while several aggregates tend to form in specimens treated with 0.13wt% of MWCNTs (Figure 6c). At 0.05 wt% the fillers distribute more homogeneously along the confined volume, suggesting that the swelling-assisted deposition provides enough nanotubes to form continuous paths without promoting their collapse into aggregates. This morphology is consistent with the improved electrical stability observed later in the piezoresistive tests (Figure 6b). The specimen with 0.03 wt% MWCNTs exhibits an insufficient number of interconnected pathways to form a stable conductive network, indicating that the filler content lies below the effective percolation threshold for this confined architecture. Conversely, at 0.13 wt% the excessive nanotube concentration promotes agglomeration, which locally disrupts network continuity and reduces the uniformity of electrical transport. This confirms that conductivity in confined porous architectures is governed by a narrow balance between filler availability and aggregation phenomena, explaining why the intermediate content (0.05 wt%) provides the most efficient percolative structure. The optimal balance between the percolative network and improved dispersion of MWCNTs is achieved with the formic-acid dispersion containing 0.2wt% of MWCNTs.

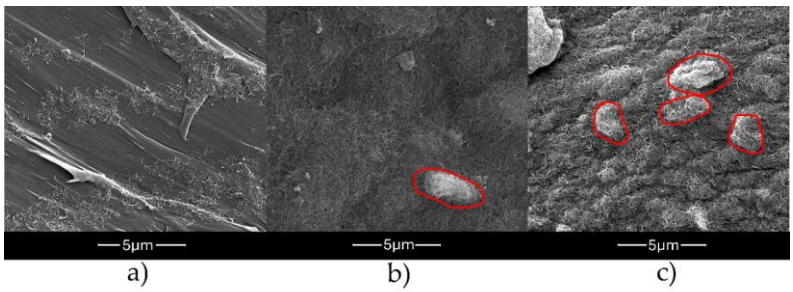

Figure 6. SEM images showing sample with a) 0.03 wt% b) 0.05 wt% c) 0.13 wt% of MWCNTs at a magnification of 25000 x, with MWCNTs aggregates highlighted in red.

3.2 Piezoresistive behaviour

Three-point cyclic bending tests were conducted to assess the behaviour of the composite material in terms of the change in electrical resistance. The strain of the specimen in the three-point bending configuration was calculated according to the following equation (1) [35]:

$$\varepsilon = \frac{6Dd}{L^2} \quad (1)$$

where D is the thickness of the tested specimen (9 mm in this case), d is the maximum deflection at the centre of the specimen, and L is the span (80 mm).

All specimens display an initial conditioning stage, attributable to viscoelastic accommodation of PA6 and to the progressive stabilization of the MWCNT contact network under cyclic bending. This transient reduces the variability of the electrical signal over the first cycles and is consistent with typical relaxation effects in semicrystalline polyamides. The electrical resistance responds to this phenomenon as shown in Figure 7. It was observed that an increase in longitudinal strain corresponded to a decrease in electrical resistance. The qiGF/0.05wt% sample follows the flection cycle very well. On the other hand, the sample longGF/0.03wt%, produced very noisy output resistance measurements. This noise is attributed to the insufficient percolation paths, as shown by SEM images. In general, the resistance signal becomes smoother and more consistent in following the strain profile (Figure S3). The periodic resistance response observed in Figure 7 originates from the reversible deformation of the confined MWCNT network under cyclic bending. The sinusoidal displacement periodically modulates the three-dimensional conductive network of MWCTS due to tunneling and micro-contacts between nanotubes. Under the limited strain range applied in tested range (0.2–0.83%), the deformation of the conductive pathways remains within the elastic regime, resulting in a stable and repeatable periodic resistance fluctuation. The small amplitude of the oscillation reflects the confined architecture of the filler network, which minimizes large-scale rearrangements and

enhances signal repeatability. The relatively small absolute resistance variation observed (approximately 2.25-2.33 kΩ), the sensor provides practical relevance in applications where low-strain detection, high stability, and minimal noise are required. The confined-network design induces resistance changes that are small in magnitude but highly repeatable.

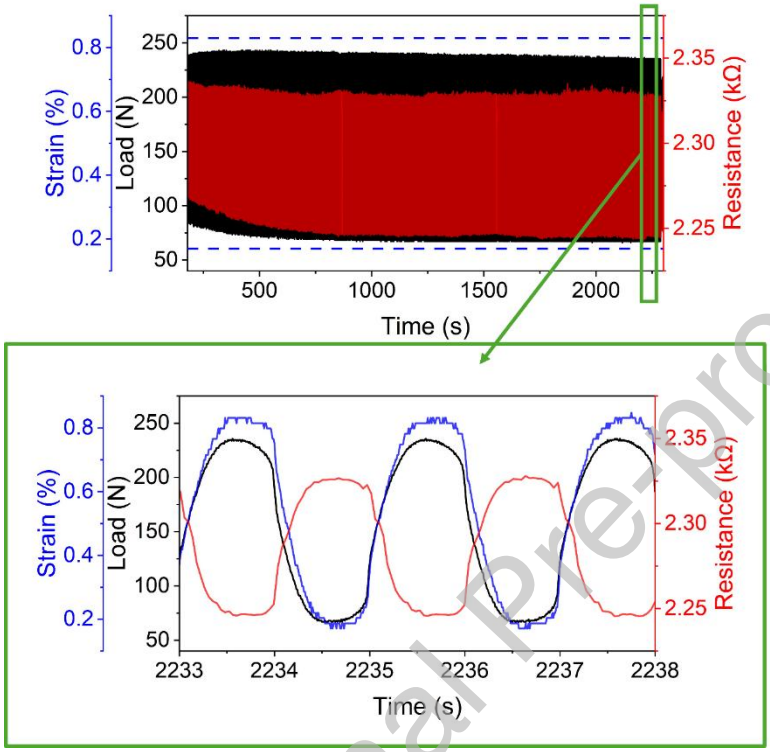

Figure 7. Load (black), strain (blue) and electrical resistance (red) cycles of the qiGF/0.05wt% specimen. The dotted lines represent the minimum and the maximum strain used as control in cyclic three-point bending tests.

Table 1 shows the maximum load and the resistance span of the several specimens. The values are calculated from the response to cyclic flection after stabilisation. The Working Range (WR) of a piezoresistive sensors is measured from the electrical resistance values at maximum strain (R_{min}) and at rest (R_0) according to the equation (2) [36]:

$$WR = R_0 - R_{min} \qquad (2)$$

Table 1 shows the nominal electrical resistance of each specimen measured at rest, after the sensor has been exercised, and the resulting WR. The resistances R_0 are all within 6 kΩ, except for the qiGF/0.03wt% and qiGF/0.13wt% samples. These discrepancies likely arise from local variations in pore closure and solvent-driven nanotube deposition during the swelling-drying step, which can modulate the effective cross-section of the conductive path. Such sensitivity to processing conditions is typical of segregated architectures, where minor differences in local compaction significantly affect baseline resistance. A similar explanation may account for a certain degree of variance between the resistances of samples with the same MWCNTs content. All other values seem to be in line with the expectation that the resistance value decreases as the filler content increases. LongGF/0.05wt%, although not having the best WR value, has an R_0 value that places it within the range of conductive materials and can therefore be considered an optimum result.

Table 1. Maximum load and resistance range of the tested specimens.

Fibre configuration	MWCNTs content of preliminary dispersion	Max load (N)	R_0 (Ω)	Working Range (Ω)
noGF	0.03 wt%	115 ± 9	4950	85
	0.05 wt%		24375	920
	0.13wt%		5370	523
qiGF	0.03 wt%	232 ± 5	2180	102
	0.05 wt%		2359	113
	0.13wt%		3464	661
longGF	0.03 wt%	266 ± 32	1310	95
	0.05 wt%		8687	711
	0.13wt%		2533	275

When the sample flexed and deflected, a gradual relaxation is observed (Figure 8) due to viscoelastic relaxation of the polymer [37]. Thus, while the machine applies a step deformation at constant loads, the load cell and multimeter record the relaxation of the polymer matrix in terms of load and change of electrical resistance.

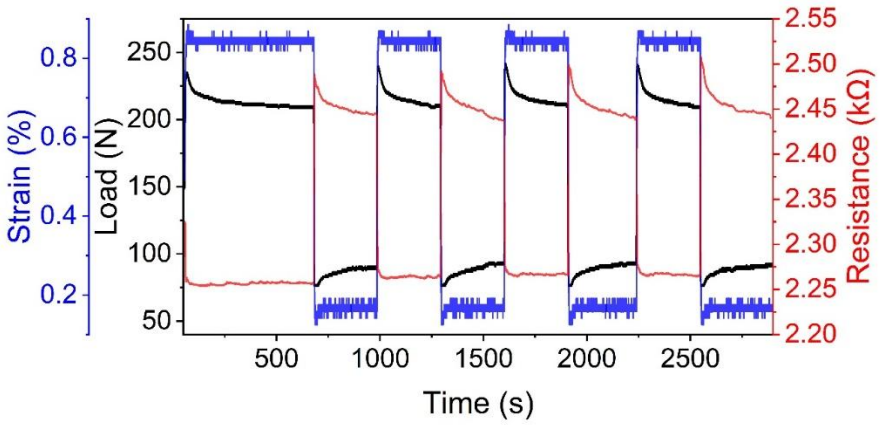

Figure 8. Creep/recovery test results for the longGF/0.13wt% sample, with curves of strain (blue), load (black), and electrical resistance (red).

The Gauge Factor (GF) is one of the most relevant parameters for a strain sensor, and it was computed as follows [17], [36]:

$$GF = \frac{(R - R_0)/R_0}{\varepsilon} \quad (3)$$

where R_0 is the electrical resistance at rest, R is the electrical resistance at the point of evaluation and ε is the strain at the point of evaluation. GFs are calculated for each sample at the maximum strain of testing, e.g. 0.83%, corresponding to a 1.0 mm displacement of the pin in the three-point-bending configuration. R, measured at the maximum strain, corresponds to the minimum resistance measured during testing.

The maximum GF of 23.06 was obtained for the longGF/0.05 wt% specimen. The observed trend reported in Figure 9a highlights the interplay between filler concentration, network morphology and fibre reinforcement. At 0.03 wt% MWCNT content the conductive network is dominated by discontinuous paths, which limits the strain-induced modulation of resistance and results in lower GF values. Increasing the filler content improves the density of percolative

pathways, thereby amplifying the resistance variation under mechanical deformation and leading to higher sensitivity.

The performance of the longGF specimens can be attributed to the alignment of the continuous glass fibres along the main loading direction, which stabilizes the strain transfer to the confined MWCNT network and promotes a more uniform compression of the conductive domains during bending. This configuration enhances the strain-dependent rearrangement of CNT contacts and tunnelling distances, producing a larger resistance change for the same applied strain. Notably, the 0.05 wt% filler content provides the most favourable balance between network continuity and avoidance of aggregation, explaining why the longGF/0.05 wt% sample exhibits the highest GF among all tested configurations.

In literature, it is possible a comparison with similar composites as structures studied by Reddy et al. [37] having two films containing CNTs loadings of 0.05 wt% and 0.1 wt%, respectively, achieved GFs of 3.8 and 7.3, at 1% strain. A similar result to the one achieved is also reported by Mahmoud et al. [38] for a 0.09 wt% graphene-doped polysilicon sensor, exhibiting a linear increase of the relative resistance of 20.1, although experiment was performed within in the range of 0÷22% strain. The approach of Kuzsella et al. [39] exploited the synergistic effect of carbon nanotubes and carbon black (CB) as nanofillers when preparing polyurethane foam pressure sensors. Their research found that the combination of 7:3 CNT:CB with a filler content of 0.44 wt% performed best, achieving a GF of 25 in the range of 0.0÷1.8% strain. Moreover, Wang et al. [40] achieved a GF of approximately 14 at 0.8% strain with their conventional sensing samples fabricated at 0.2 vol%.

The comparison with the literature suggest that the confinement approach used in this work effectively promotes the formation of a well-segregated and continuous conductive network, thereby improving electrical transport even at low MWCNT loadings. The resulting gauge

factors demonstrate the efficiency of this segregated architecture in amplifying strain-induced variations in conduction.

To assess the electrical response linearity of the printed composite sensors, electrical resistance data at five strain values was averaged over a period corresponding to five cycles. R^2 was calculated from the line fitting the obtained data on the R/strain chart [42]. Fiber reinforcement has a negligible effect on the linearity of the measurements, with the filler content playing a more prominent role (Figure 9b). In fact, in line with literature [43], the results show an initial improvement moving from samples obtained with 0.03 wt% MWCNTs to treated with 0.05 wt% MWCNTs and a further improvement for samples obtained by using the MWCNTs at 0.13 wt% specimens (Figure S4).

Hysteresis in piezoresistive sensors refers to the difference in the output signal between loading and unloading cycles for the same applied mechanical input (i.e. without bending/deformation) For all samples hysteresis was measured according to the method reported by Liang et al. [36]. Specifically, data points were collected along five cycles of deformation. The five data points considered were those corresponding to 0.2, 0.4, 0.6, 0.8, and 1.0 mm displacements.

The hysteresis appeared smaller for samples with high filler contents and, interestingly, the reduction in error was significant only between the 0.03 wt% and 0.05 wt% specimens (reaching 68.1% reduction in the qiGF specimens), while the reduction between 0.05 wt% and 0.13 wt% was negligible (Figure 9c). The best performance was achieved by the longGF/0.13wt% specimen. Overall, as shown in Figure 9b, the continuous fiber reinforcement was shown to decrease the hysteresis error.

Repeatability describes the degree of consistency between measurement results under the same conditions [44]. As an indicator of repeatability, is the Error of Full Scale, which is defined as the maximum deviation of the actual sensor output from the ideal response, expressed as a

percentage of the full-scale output range. This parameter represents the worst-case total error expected across the entire operating range of the sensor [45], and is expressed as indicated in Equation (4). From the creep/recovery test data, a set of four measurements was taken for each cycle at maximum strain. The average was calculated for each cycle and later used as the reference measurement for that cycle. The feature was calculated as the mean of the measurements of all cycles for each specimen.

$$\%\, Error\ of\ Full\ Scale = \frac{Measurement - Reference}{Full\ Scale} * 100 \qquad (4)$$

Figure 9d shows that the error decreases with increasing filler content. In addition, the error between different measurements is reduced in the reinforced specimens in the case of 0.03 wt% and 0.05 wt% filler content. The best performance is obtained at high filler loading. On the other hand, the presence and orientation of the reinforcement contribute to reducing the error rate, with the best results achieved by the longGF. The improved repeatability in fibre-reinforced specimens, particularly at intermediate filler content, may stem from the ability of continuous fibres to constrain matrix deformation and limit irreversible sliding at the interface between polymer and conductive the filler. By stabilizing the mechanical strain field, the fibres reduce cycle-to-cycle drift and preserve the integrity of the conductive network during repeated loading, preventing its irreversible absorption by the polymer matrix and subsequent loss.

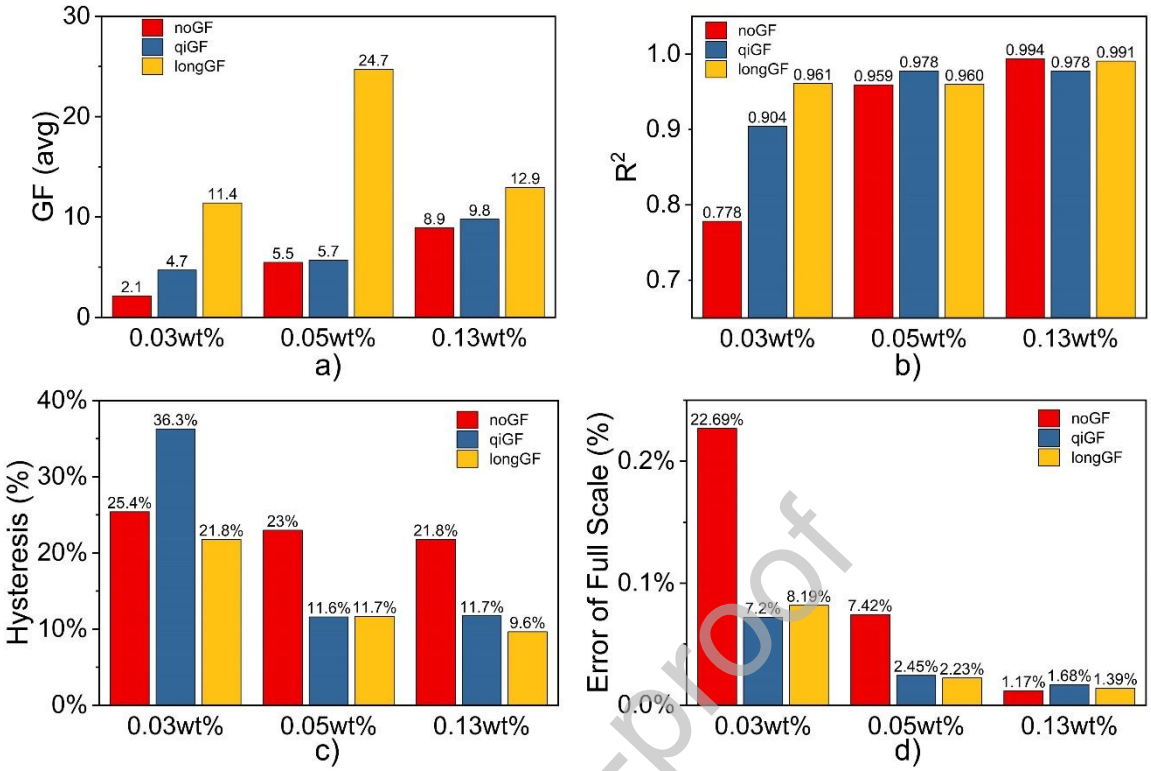

Figure 9. Comparison for noGF (red), qiGF (blue), and longGF (yellow) samples about a) GF, b) R^2, c) Hysteresis, and d) Error full scale values.

The creep/recovery behaviour, including the Root-Mean-Square Error (RMSE) and the sensitivity was evaluated by Liang's group for their sensors [46]. Considering the linear part of the response, they calculated the RMSE as index of the noise of the response and also calculated the sensitivity as slope of the fitted linear response. As each sample had a different base electrical resistance, RMSE values were normalized with the average resistance in the considered interval of values. Similarly, the evaluation procedure was repeated from data related at 0.83% strain (nominal 1.0 mm deflection) and 0.21% strain (nominal 0.2 mm deflection).

Usually the absolute slope values are greater when the creep/recovery test response is that at lower strain (0.21%), because the stress inside the sensor material is naturally decreasing in a

non-imposed way. On the contrary, in cycles at maximum strain the stress is externally imposed to the sensors. This same result was observed in [46], where the researchers concluded that it was likely because the sensors relied almost entirely on their own elastic rebound during the relaxation.

Interestingly, the sign of the slope differed by reinforcement: the noGF and qiGF specimens tended to exhibit negative slopes (resistance decaying over time), whereas the longGF specimens showed small positive slopes. Therefore, no clear trend was observed that could demonstrate the contribution of the reinforcing fiber in improving the drift behavior at the end of each creep/recovery cycle. This suggests that the fibreglass reinforcement did not significantly stabilize the steady-state resistance signal. For example, the most stable specimen at maximum strain results the noGF/0.13wt% with a slope of $-3.45 \cdot 10^{-6}$, while the noGF/0.03wt% with $-1.47 \cdot 10^{-4}$ slope value resulting the worst performing.

The noise (normalized RMSE) during the creep/recovery cycle was generally lower at 0.83% strain than at 0.21%, meaning the sensors were less noisy at higher strain levels. Somewhat unexpectedly, the non-reinforced specimens had the lowest noise: the noGF/0.13wt% sample was the noisiest with a normalized RMSE of ~0.002%, whereas the longGF/0.03wt% was the noisiest with ~0.501% (Table S1 and Table S2). This indicates that in terms of fine steady-state precision, the fibreglass reinforcement did not provide a benefit and may have introduced slight additional noise (possibly due to fibreglass/polymer interface effects under sustained strain). Nonetheless, at higher filler contents all configurations showed very low noise levels, demonstrating the viability of these materials for stable sensing under static loads.

4 Conclusions

The present work demonstrated the feasibility of a 3D-printed fibreglass-reinforced PA6 composite with confined MWCNTs as a strain-sensing material. A porous PA6 sandwich

structure was designed and fabricated via FDM. The internal channels were filled with a formic acid/MWCNT dispersion, and hot-pressed to embed a MWCNTs conductive network inside the polyamide matrix. The resulting specimens were subjected to three-point bending tests under both cyclic and static bending, which revealed a clear correlation between applied strain and electrical resistance. The electrical resistance of the composites ranges from approximately 1 to 9 kΩ, and the gauge factor depends on filler content and fibre reinforcement reaching a maximum of about 23 at 0.83% strain in the optimal configuration. The response linearity was mainly governed by the MWCNT content, with minimal influence from the fibre reinforcement. Hysteresis errors decreased with both higher filler content and the presence of continuous fibres. Although the fibre reinforcement improved repeatability in the low-filler specimens, the same specimens exhibited slightly not linear behavior. Overall, filler content proved to be the critical parameter for sensor performance, while continuous fibreglass reinforcement was beneficial for reducing hysteresis and improving cyclic repeatability. Among the tested compositions, the 0.05 wt% MWCNT content offered the best balance of high gauge factor, linear response, and good repeatability, especially when combined with parallel (longitudinal) fibre reinforcement. This self-monitoring composite material offers significant advantages, including elimination of embedded sensor hardware in 3D-printed parts, improved ease of product testing, and real-time strain monitoring in lightweight aerospace components or in orthotic and prosthetic devices. Moreover, this study demonstrates for the first time that 3D-printed PA6 sandwich structures with confined MWCNTs networks can serve as effective self-sensing materials, exhibiting stable piezoresistive behaviour without the need for external sensors.

The self-sensing PA6 sandwich structure reinforced with continuous fibreglass and incorporating a confined MWCNT network shows clear potential for practical applications in low-strain structural health monitoring. The combination of lightweight construction, low-noise electrical response and high gauge factor makes these materials suitable for real-time

monitoring of 3D-printed composite parts, load-bearing lightweight elements in aerospace and mobility, and embedded sensing in prosthetic and orthotic devices where deformation levels are small but repeatability is crucial.

Acknowledgments

The authors gratefully acknowledge the support of the iENTRANCE@ENL - Infrastructure for ENergy TRAnsition aNd Cir-cular Economy @Eu-roNanoLab with grant IR PNRR IR0000027, and ISIS@MACH ITALIA Research Infrastructure, the hub of ISIS Neutron and Muon Source (UK), [MUR official registry U. 0008642.28-05-2020 – 16th April 2020]. IM@IT is listed in the Italian Ministry of University and Research's Piano Nazionale delle Infrastrutture di Ricerca (PNIR 2021-2027) "in the broader notion of ISIS", and ISIS Facility and IM@IT are jointly listed in high priority RI's (see Table 6 page 30, note 38, PNIR in 2021-2027). The authors acknowledge financial support under the National Recovery and Resilience Plan (NRRP), Mission 4, Component 2, Investment 1.1, Call for tender No. 104 published on 2.2.2022 by the Italian Ministry of University and Research (MUR), funded by the European Union – NextGenerationEU– Project Title "Integration of Continuous Fibers and Self-healing Agents in 3D Printed Thermoplastic Composites" (INFINITE) – CUP B53D23008690006 - Grant Assignment Decree No. 1389 adopted on 01/09/2023 by the Italian Ministry of Ministry of University and Research (MUR).

Data Availability Statement

The authors confirm that the data supporting the findings of this study are available within the article and its supplementary materials.

Declaration of conflicts of interests

All authors hereby declare that there are no conflicts of interest.

5 References

[1] A. K. Chauhan, A. Singh, D. Kumar, and K. Mishra, "Properties of Composite Materials," in *Composite Materials*, First edition. | Boca Raton, FL : CRC Press, 2021.: CRC Press, 2021, pp. 61–78. doi: 10.1201/9781003080633-3.

[2] Compositi Magazine, "Nanocompositi 'self-sensing' per il monitoraggio dell'integrità strutturale di componenti in composito."

[3] S. Laflamme and F. Ubertini, "Back-to-Basics: Self-Sensing Materials for Nondestructive Evaluation."

[4] P. M. Ferreira, M. A. Machado, M. S. Carvalho, and C. Vidal, "Embedded Sensors for Structural Health Monitoring: Methodologies and Applications Review," Nov. 01, 2022, *MDPI*. doi: 10.3390/s22218320.

[5] K. Ramachandran, P. Vijayan, G. Murali, and N. I. Vatin, "A Review on Principles, Theories and Materials for Self Sensing Concrete for Structural Applications," Jun. 01, 2022, *MDPI*. doi: 10.3390/ma15113831.

[6] P. M. Ferreira, M. A. Machado, M. S. Carvalho, and C. Vidal, "Embedded Sensors for Structural Health Monitoring: Methodologies and Applications Review," Nov. 01, 2022, *MDPI*. doi: 10.3390/s22218320.

[7] J. A. King, D. R. Klimek, I. Miskioglu, and G. M. Odegard, "Mechanical properties of graphene nanoplatelet/epoxy composites," *J Compos Mater*, vol. 49, no. 6, pp. 659–668, Mar. 2015, doi: 10.1177/0021998314522674.

[8] K. H. Kim, J. U. Jang, G. Y. Yoo, S. H. Kim, M. J. Oh, and S. Y. Kim, "Enhanced Electrical and Thermal Conductivities of Polymer Composites with a Segregated Network of Graphene Nanoplatelets," *Materials*, vol. 16, no. 15, Aug. 2023, doi: 10.3390/ma16155329.

[9] W. Luheng, D. Tianhuai, and W. Peng, "Influence of carbon black concentration on piezoresistivity for carbon-black-filled silicone rubber composite," *Carbon N Y*, vol. 47, no. 14, pp. 3151–3157, Nov. 2009, doi: 10.1016/J.CARBON.2009.06.050.

[10] B. Düsenberg *et al.*, "Production and analysis of electrically conductive polymer - Carbon-black composites for powder based Additive Manufacturing," in *Procedia CIRP*, Elsevier B.V., 2022, pp. 18–22. doi: 10.1016/j.procir.2022.08.107.

[11] A. Nag, M. E. E. Alahi, S. C. Mukhopadhyay, and Z. Liu, "Multi-walled carbon nanotubes-based sensors for strain sensing applications," Feb. 02, 2021, *MDPI AG*. doi: 10.3390/s21041261.

[12] M. U. Azam, A. Schiffer, and S. Kumar, "Piezoresistive behavior of MWCNT/PA12 honeycomb composites processed via selective laser sintering," *Journal of Materials Research and Technology*, vol. 26, pp. 2319–2332, Sep. 2023, doi: 10.1016/j.jmrt.2023.08.051.

[13] L. Fazi *et al.*, "Characterization of Conductive Carbon Nanotubes/Polymer Composites for Stretchable Sensors and Transducers," *Molecules*, vol. 28, no. 4, Feb. 2023, doi: 10.3390/molecules28041764.

[14] I. L. Hia, A. D. Snyder, J. S. Turicek, F. Blanc, J. F. Patrick, and D. Therriault, "Electrically conductive and 3D-printable copolymer/MWCNT nanocomposites for strain sensing," *Compos Sci Technol*, vol. 232, Feb. 2023, doi: 10.1016/j.compscitech.2022.109850.

[15] G. Rollo *et al.*, "On the synergistic effect of multi-walled carbon nanotubes and graphene nanoplatelets to enhance the functional properties of SLS 3D-printed elastomeric structures," *Polymers (Basel)*, vol. 12, no. 8, Aug. 2020, doi: 10.3390/POLYM12081841.

[16] S. H. Park *et al.*, "Modeling the electrical resistivity of polymer composites with segregated structures," *Nat Commun*, vol. 10, no. 1, Dec. 2019, doi: 10.1038/s41467-019-10514-4.

[17] S. Tadakaluru, W. Thongsuwan, and P. Singjai, "Stretchable and flexible high-strain sensors made using carbon nanotubes and graphite films on natural rubber," *Sensors (Switzerland)*, vol. 14, no. 1, pp. 868–876, Jan. 2014, doi: 10.3390/s140100868.

[18] A. Nag, M. E. E. Alahi, S. C. Mukhopadhyay, and Z. Liu, "Multi-walled carbon nanotubes-based sensors for strain sensing applications," Feb. 02, 2021, *MDPI AG*. doi: 10.3390/s21041261.

[19] M. Salzano de Luna *et al.*, "Nanocomposite polymeric materials with 3D graphene-based architectures: from design strategies to tailored properties and potential applications," *Prog Polym Sci*, vol. 89, pp. 213–249, Feb. 2019, doi: 10.1016/J.PROGPOLYMSCI.2018.11.002.

[20] Ian Gibsonn, David Rosen, and Brent Stucker, "Additive Manufacturing Technologies," 2021.

[21] A. Ambrosi and M. Pumera, "3D-printing technologies for electrochemical applications.," *Chem Soc Rev*, vol. 45 10, pp. 2740–55, 2016, [Online]. Available: https://api.semanticscholar.org/CorpusID:205960563

[22] H. Guo, R. Lv, and S. Bai, "Recent advances on 3D printing graphene-based composites," *Nano Materials Science*, vol. 1, no. 2, pp. 101–115, Jun. 2019, doi: 10.1016/j.nanoms.2019.03.003.

[23] Y. Liu and S. L. Sing, "A review of advances in additive manufacturing and the integration of high-performance polymers, alloys, and their composites," *Materials Science in Additive Manufacturing*, vol. 2, no. 3, p. 1587, Sep. 2023, doi: 10.36922/msam.1587.

[24] S. M. F. Kabir, K. Mathur, and A. F. M. Seyam, "A critical review on 3D printed continuous fiber-reinforced composites: History, mechanism, materials and properties," Jan. 15, 2020, *Elsevier Ltd*. doi: 10.1016/j.compstruct.2019.111476.

[25] F. Mashayekhi, J. Bardon, V. Berthé, H. Perrin, S. Westermann, and F. Addiego, "Fused filament fabrication of polymers and continuous fiber-reinforced polymer composites: Advances in structure optimization and health monitoring," Mar. 01, 2021, *MDPI AG*. doi: 10.3390/polym13050789.

[26] P. Cheng *et al.*, "3D printed continuous fiber reinforced composite lightweight structures: A review and outlook," *Compos B Eng*, vol. 250, Feb. 2023, doi: 10.1016/j.compositesb.2022.110450.

[27] F. Lupone, E. Padovano, C. Venezia, and C. Badini, "Experimental Characterization and Modeling of 3D Printed Continuous Carbon Fibers Composites with Different Fiber Orientation Produced by FFF Process," *Polymers (Basel)*, vol. 14, no. 3, Feb. 2022, doi: 10.3390/polym14030426.

[28] E. H. Saidane, G. Arnold, P. Louis, and M. J. Pac, "3D printed continuous glass fibre-reinforced polyamide composites: Fabrication and mechanical characterisation," *Journal of Reinforced Plastics and Composites*, vol. 41, no. 7–8, pp. 284–295, Apr. 2022, doi: 10.1177/07316844211051746.

[29] P. Cheng *et al.*, "3D printed continuous fiber reinforced composite lightweight structures: A review and outlook," *Compos B Eng*, vol. 250, Feb. 2023, doi: 10.1016/j.compositesb.2022.110450.

[30] F. Mashayekhi, J. Bardon, V. Berthé, H. Perrin, S. Westermann, and F. Addiego, "Fused filament fabrication of polymers and continuous fiber-reinforced polymer composites: Advances in structure optimization and health monitoring," Mar. 01, 2021, *MDPI AG*. doi: 10.3390/polym13050789.

[31] Y. Wang *et al.*, "3D-printing of segregated carbon nanotube/polylactic acid composite with enhanced electromagnetic interference shielding and mechanical performance," *Mater Des*, vol. 197, Jan. 2021, doi: 10.1016/j.matdes.2020.109222.

[32] R. 3-10/10/2023 markforged.com, "Material Datasheet," 2023.

[33] Y. Liu, J. Li, and Z. J. Pan, "The dispersion of CNT and the conductive property of PA6/MWNTs nanofiber filaments by electrospinning," in *Advanced Materials Research*, 2011, pp. 1993–1997. doi: 10.4028/www.scientific.net/AMR.295-297.1993.

[34] F. M. Monticeli, H. L. OrnaghiJr, R. M. Neves, and M. O. H. Cioffi, "Creep/recovery and stress-relaxation tests applied in a standardized carbon fiber/epoxy composite: Design of experiment approach," *J Strain Anal Eng Des*, vol. 55, no. 3–4, pp. 109–117, 2020, doi: 10.1177/0309324719892710.

[35] "Standard Test Methods for Flexural Properties of Unreinforced and Reinforced Plastics and Electrical Insulating Materials 1." [Online]. Available: www.astm.org

[36] A. Liang, R. Stewart, and N. Bryan-Kinns, "Analysis of sensitivity, linearity, hysteresis, responsiveness, and fatigue of textile knit stretch sensors," *Sensors (Switzerland)*, vol. 19, no. 16, Aug. 2019, doi: 10.3390/s19163618.

[37] G. Rollo, A. Ronca, P. Cerruti, H. Xia, E. Gruppioni, and M. Lavorgna, "Optimization of Piezoresistive Response of Elastomeric Porous Structures Based on Carbon-Based Hybrid Fillers Created by Selective Laser Sintering," *Polymers (Basel)*, vol. 15, no. 22, Nov. 2023, doi: 10.3390/polym15224404.

[38] S. K. Reddy, S. Kumar, K. M. Varadarajan, P. R. Marpu, T. K. Gupta, and M. Choosri, "Strain and damage-sensing performance of biocompatible smart CNT/UHMWPE nanocomposites," *Materials Science and Engineering C*, vol. 92, pp. 957–968, Nov. 2018, doi: 10.1016/j.msec.2018.07.029.

[39] W. E. Mahmoud and S. A. Al-Bluwi, "Development of ultrasensitive mechanical strain sensor made of 2D-assembled graphene monolayers aligned parallel into polysilicon nanocomposites," *Sens Actuators A Phys*, vol. 313, Oct. 2020, doi: 10.1016/j.sna.2020.112166.

[40] M. Nabeel, L. Kuzsella, B. Viskolcz, M. Kollar, B. Fiser, and L. Vanyorek, "Synergistic effect of carbon nanotubes and carbon black as nanofillers of silicone rubber pressure sensors," *Arabian Journal of Chemistry*, vol. 16, no. 4, Apr. 2023, doi: 10.1016/j.arabjc.2023.104594.

[41] M. Wang *et al.*, "Enhanced electrical conductivity and piezoresistive sensing in multi-wall carbon nanotubes/polydimethylsiloxane nanocomposites: Via the construction of a self-segregated structure," *Nanoscale*, vol. 9, no. 31, pp. 11017–11026, Aug. 2017, doi: 10.1039/c7nr02322g.

[42] H. Jung, C. Park, H. Lee, S. Hong, H. Kim, and S. J. Cho, "Nano-cracked strain sensor with high sensitivity and linearity by controlling the crack arrangement," *Sensors (Switzerland)*, vol. 19, no. 12, Jun. 2019, doi: 10.3390/s19122834.

[43] Bouhamed Ayda, Sun Xin, and Kanoun Olfa, "Optimization of MWCNTs/Epoxy for High Strain Sensor Performance," 2019.

[44] V. K. Samoei, A. H. Jayatissa, and K. Sano, "Flexible Pressure Sensor Based on Carbon Black/PVDF Nanocomposite," *Chemical Science International Journal*, vol. 33, no. 2, pp. 1–10, Feb. 2024, doi: 10.9734/csji/2024/v33i2885.

[45] Texas Instruments, "Sensor accuracy error and repeatability." Accessed: Mar. 02, 2024. [Online]. Available: https://www.ti.com/video/6031597003001

[46] A. Liang, R. Stewart, and N. Bryan-Kinns, "Analysis of sensitivity, linearity, hysteresis, responsiveness, and fatigue of textile knit stretch sensors," *Sensors (Switzerland)*, vol. 19, no. 16, Aug. 2019, doi: 10.3390/s19163618.

Declaration of Interest Statement

☒ The authors declare that they have no known competing financial interests or personal relationships that could have appeared to influence the work reported in this paper.